Deflected Capillary Force Lithography

Yangjun Cai, Zhi Zhao, Jixin Chen, Tinglu Yang, and Paul S. Cremer*

Department of Chemistry, Texas A&M University, P.O. Box 30012, College Station, Texas 77843, United States

ABSTRACT Herein we introduce a novel strategy based on capillary force lithography (CFL) to fabricate asymmetric polymeric ring structures by applying both shear and nomal forces to a poly(dimethylsiloxane) stamp. The mechanism for the formation of asymmetric rings is caused by the deflection of cylindrical PDMS pillars due to the shear load, which is therefore termed deflected CFL (dCFL). The asymmetric polymeric rings could be readily transferred to an underlying gold layer to generate split ring structures with tunable opening angles. Asymmetric structures based upon trigular and square-shaped pillars were also fabricated. These elements were formed into periodic arrays over surface areas as large as 1 cm^2 and may have optical and electromagnetic applications.

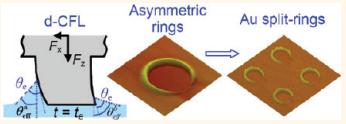

KEYWORDS: capillary force lithography · capillary rise · split ring · asymmetric nanostructure · soft lithography · PDMS

Patterned arrays of metallic nanostructures have attracted substantial interest due to their optical and electromagnetic properties. Specifically, anisotropic nanostructures with reduced symmetry, such as split rings (C, L, and U-shapes)[1−3] or crescents,[4] exhibit unique optical and electromagnetic properties compared to their symmetric analogues. Anisotropic nanostructures have been developed for negative index materials (NIMs),[3,5,6] localized surface plasmon resonance (LSPR) spectroscopy,[7] chemical and biological sensors,[1,8,9] surface-enhanced Raman scattering (SERS),[10] frequency-selective surfaces (FSS),[2] and magnetic materials.[11]

Typically, anisotropic nanostructures have been fabricated by electron beam lithography (EBL).[9] However, EBL is time-consuming and relatively expensive. In fact, the fabrication process is generally impractical for patterning areas on the scale of 1 cm^2. Alternatively, shadow nanosphere lithography has emerged as a simple and cost-effective technique for large-scale fabrication of metal crescents.[4,12] Since the crescents originate from arrayed nanospheres, this technique is mostly restricted to generating anisotropic structures with circular geometries. Recently, another alternative technique involving nanoskiving in combination with shadow evaporation has overcome this limitation.[2,13] Because nanoskiving is based on prefabricated patterns, it can generate anisotropic structures with various geometries, including circular, L- and U-shaped split rings. As such, this technique is quite versatile. However, the key procedure for this method, sectioning by microtome, requires experienced users to section the patterns.[14] Tilted nanoimprinting lithography (t-NIL) has also been used to create split ring structures with limited control over the geometry of the features.[15]

Herein, we report a simple capillary force lithography method for generating anisotropic metallic nanostructures. The technique allows for the formation of shapes with tunable angular and directional properties. The method works *via* the deflection of PDMS pillars during the CFL process to generate asymmetric polymer structures. Traditional CFL is based on the thermally mediated capillary rise of a polymer melt along the sidewalls of an elatomeric polydimethylsiloxane (PDMS) mold.[16,17] This would lead to symmetric replication of the contours of the PDMS mold under a normal load (Figure 1a). However, we have found that asymmetric replication could be performed by introducing an additional shear load without the use of any specialized equipment. Such shear can be applied simply by placing a wedge with slope ω on top of the PDMS mold and applying a load to it with a heavy object such as an iron block (Figure 1b). The asymmetric polymer structures can be exploited to generate anisotropic metallic structures by combining this procedure with reactive ion etching (RIE) and subsequent chemical etching. Since CFL is a variant of soft lithography, the method possesses the associated advantages, such as low-cost, high-throughput, and the ability to pattern macroscopic areas. Moreover, metallic structures with 100 nm scale features can be made with periodicities on the scale of a few micrometers or less.

* Address correspondence to cremer@mail.chem.tamu.edu.

Received for review November 21, 2011 and accepted December 21, 2011.

Published online January 06, 2012
10.1021/nn2045278

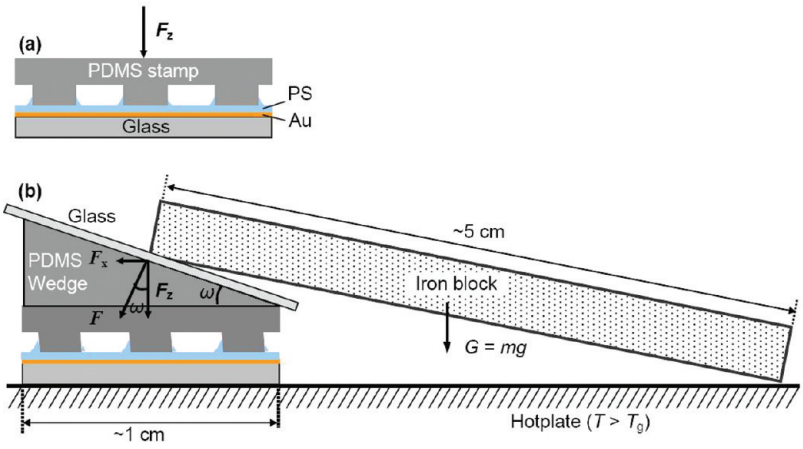

Figure 1. Schematic illustration of the setup of CFL (a) and dCFL (b). CFL is performed under a normal force (F_z). By contrast, dCFL is performed under both shear (F_x) and normal (F_z) forces, which are introduced by adding a PDMS wedge (wedge angle, ω, ~20°) onto the PDMS stamp. The force is applied by an iron block (mass, m) that touches both a glass slide-covered PDMS wedge as well as a hot plate. The temperature of the hot plate (T) is set above T_g of the PS film. The gravitational force of the iron block is G (= mg, where g is the accelaration due to gravity).

RESULTS

Deflected capillary force lithography can be performed by a simple benchtop procedure. The experimental method involves bringing a PDMS stamp into conformal contact with a 50 nm thick polystyrene (PS) film (M_w = 97.4 kDa) spin-coated onto a 50 nm thick Au film on glass. The system was then annealed at 130 °C for 30 min. This is significantly above the glass transition temperature of PS ($T_g \approx 100$ °C). The PDMS stamps employed were *ca.* 1 cm × 1 cm and contained a square array of cylindrical pillars (Supporting Information, Figure S1). As a control, CFL was first carried out under a normal compressive force ($F_z \approx 1.2$ N) (Figure 1a). The AFM image and the line profile for this case show that circular PS rings were formed on a Au surface (Figure 2a). Next, dCFL was carried out with a combined shear (F_x) and normal (F_z) force as depicted schematically in Figure 1b. This was done by placing a PDMS wedge with an angle, ω, of 20° onto the PDMS stamp. An iron block was bridged between the wedge and a hot plate onto which the substrate was placed (Figure 1b). As shown in the schematic diagram, F_z is the normal force, while F_x is the force parallel to the PDMS/PS interface. The normal force was the same as in the control expriment (~1.2 N) and F_x was ~0.4 N. This produced PS rings of asymmetric height upon applying the force at 130 °C for 30 min (Figure 2b). The line profile from the AFM image reveals that the maximun height of the capillary rise, h_{max}, was 155 ± 6 nm, while on the opposite side, h_{min}, the value was only 36 ± 6 nm. The asymmetric PS rings were fabricated over large areas (typically 1 cm × 1 cm) as shown in Figure S2 in the Supporting Information.

The driving force for the capillary rise in CFL is the Laplace pressure created by the curved interface. The initial contact angle, θ_0, between the PDMS and the PS

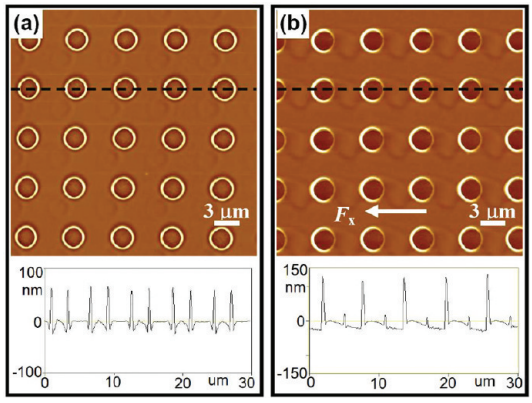

Figure 2. AFM images and corresponding line profiles of symmetric (a) and asymmetric (b) PS rings fabricated by normal CFL and dCFL, respectively. The white arrow in panel b indicates the direction of F_x. The dashed black lines in the micrographs represent the positions over which the line profiles were measured.

film (typically ~90° under a normal compressive force if the PDMS wall is vertical) is larger than the equilibrium contact angle (θ_e) of the PS melt on the PDMS surface.[16,17] This angle changes constantly over the course of an experiment until equilibrium is approached. The driving force for capillary wetting can be expressed as: $F_w = \gamma_{PS}(\cos\theta_e - \cos\theta_t)$, where θ_t is the dynamic contact angle of the PS melt on the PDMS surface.[18] A capillary rise, U, typically occurs over the time scale of a few hours before equilibrium is finally achieved. U is determined at the three-phase contact line (PS/PDMS/air) by θ_t and is directly proportional to F_w as

$$U \cong \frac{\gamma_{PS}(\cos\theta_e - \cos\theta_t)}{\zeta_0 + 72\eta/\tan\theta_t} \quad (1)$$

where ζ_0 is the coefficient of the contact-line friction and η is the viscosity of the PS melt.[18] For PS with

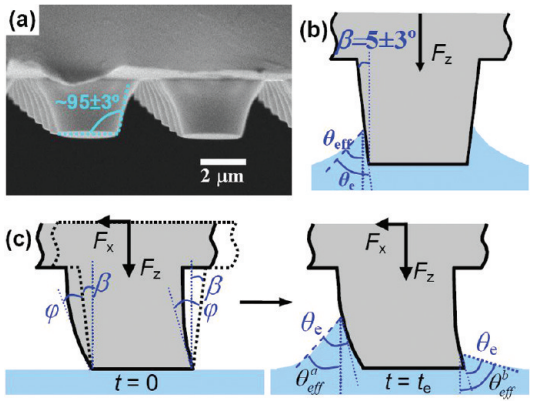

Figure 3. (a) Cross-sectional SEM image of a typical PDMS stamp with cylindrical pillars. The walls of each pillar make an angle of 95 ± 3° with respect to the flat end of the pillar. (b) Schematic illustration of the equilibrium state in standard CFL. θ_e is the equilibrium contact angle of the PS melt on PDMS (~76°). θ_{eff} is the effective equilibrium contact angle. β (5 ± 3°) is the tilt angle of the PDMS wall with respect to the vertical line. Under a vertical force (F_z), the capillary rise is identical all around the pillar. (c) Schematic illustration of the mechanism for the formation of the asymmetric PS rings in dCFL. φ is the deflection angle of the PDMS pillar under the combined loads of F_x and F_z. θ^a_{eff} and θ^b_{eff} are the effective equilibrium contact angles on the left and right sides of the pillars ($\theta^a_{eff} < \theta_e < \theta^b_{eff}$).

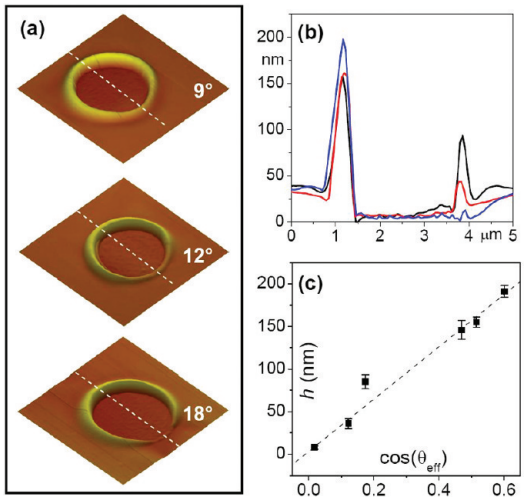

Figure 4. (a) 3-D AFM images (5 μm × 5 μm) of asymmetric PS rings generated under different forces ($F \approx 330$, 449, and 624 nN on each PDMS pillar) corresponding to the three different deflection angles ($\varphi \approx 9°$, 12°, and 18°) indicated on the images. (b) Comparison of line profiles from panel (a) taken along the dashed white lines. (c) Plot of the height of the rings (h) as a function of cos(θ_{eff}).

M_w = 97.4 kDa at 130 °C, θ_e is estimated from Young's equation to be ~76°, based upon an interfacial tension of approximately 15.1 mN/m for the PDMS/air interface, 6.1 mN/m for the PDMS/PS-melt interface, and 37.3 mN/m for the PS-melt/air interface.[19] A cross-sectional SEM image of the PDMS stamp shows that the pillar wall is not strictly vertical but rather curved outward near the base (Figure 3a). Even though the pillar wall is curved, the tilt angle (β) with respect to the surface normal is still considered to be roughly constant ($\beta = 5 \pm 3°$) (Figure 3b) since the height of the capillary rise, which in this case is 155 nm at its maximum value, is far smaller than the pillar height (~2.5 μm). As a result, θ_e may be substituted by an effective equilibrium contact angle $\theta_{eff} = \theta_e - \beta$ (~71°) (Figure 3b).[20] Because $\theta_{eff} < 90°$, the PS melt will wet the walls of the PDMS pillars and capillary rise will occur.

Since only a normal force is applied in a typical CFL experiment, θ_{eff} is identical all the way around the pillar. Therefore, the capillary rise is uniform, which leads to the formation of symmetric rings (Figure 2a). However, when both shear and normal forces (F_x and F_z) are applied in dCFL, the PDMS pillars readily deflect (Figure 3c) due to the low Young's modulus of the PDMS (E = 1.0 MPa). The deflection angle (φ) can be estimated as the sum of three separate contributions: the bending angle (φ_b), the shear-induced angle (φ_s), and the base-tilting angle (φ_t) (see Supporting Information).[21] The force applied on each pillar, F, can be calculated as F_{total}/n, where F_{total} is the force applied to the stamp and n is the number of the pillars on the stamp ($n \approx 1.7 \times 10^7$ in the current case). The mass (m) of the iron block placed onto the PDMS stamp is ~245 g (F_{total} = 1.25 N). Therefore, the value of F is ~450 nN/pillar. As a result, F_x (=$F \sin \omega$) and F_z (=$F \cos \omega$) are ~160 and ~450 nN, respectively. The deflection angle, φ (=$\varphi_b + \varphi_s + \varphi_t$), is estimated to be ~12° (see Supporting Information for details of this calculation). As a result, θ_{eff} changes from ~71° in normal force CFL (Figure 3c) to ~59° ($\theta^a_{eff} = \theta_e - (\varphi + \beta)$) and ~83° ($\theta^b_{eff} = \theta_e + (\varphi - \beta)$), respectively, for the left and right sides of the pillar under the experimental conditions employed in Figure 2b. During the capillary rise in dCFL, θ_t decreases from 90° until reaching equilibrium (*i.e.*, θ^a_{eff} and θ^b_{eff}) and evolves between these angles during the interim. According to eq 1, $U_a > U_b$ because $\cos(\theta^a_{eff}) > \cos(\theta^a_{eff})$. Thus, the resuting height of the capillary rise on the left side should be greater than that on the right side. That is exactly what the AFM measurement reveals (Figure 2b).

To further confirm that the formation of asymmetric rings is due to the deflection of the PDMS pillars, we applied a variety of forces to the wedge by changing the weight of the iron block (m = 180, 245, and 345 g) to induce different deflection angles ($\varphi \approx 9°$, 12°, and 18°). Figure 4a shows the AFM images of the PS rings generated at three different forces. Figure 4b compares the line profiles from the AFM images and shows the maximum (h_{max}) and minimum (h_{min}) heights of the asymmetric rings in Figure 4a. As expected, h_{max} increases and h_{min} decreases with the increase in the applied force and the corresponding increase in the deflection angles ($\varphi \approx 9°$, 12°, and 18°). In particular, at m = 345 g (φ ~18°), θ_{eff} is ~89°, which is

close to 90°. Thus, almost no capillary rise occurs on one side. This is manifest by the near absence of polymer material at the low point of the asymmetric ring in the bottom AFM image (also Figure 4b, blue curve). The result is somewhat analogous to the effect obtained by using the tilting-plate method in contact angle measurements, where the contact angle is high on one side of the plate and nearly flat on the other.[20,22] The measured heights of the capillary rise for all three h_{max} and h_{min} values *versus* $\cos(\theta_{eff})$ are plotted in Figure 3c, showing that h increases with $\cos(\theta_{eff})$. This is in agreement with eq 1, suggesting that the calculation of the deflection angles and the experimental results are consistent.

Asymmetric PS rings generated from dCFL can be used as templates to fabricate Au structures by reactive ion etching (RIE) and subsequent wet chemical etching of the underlying Au film as depicted schematically in Figure 5.[17] Figure 6a shows an AFM image of C-shaped Au nanoarchitectures created with the template shown in Figure 2b. The opening angle, α, of these stuctures was approximately 60°. In this case, the etching time was 45 s. Rings with an opening angle of 120° can be created with an etching time of 65 s (Figure 6b). This angle could be continuously controlled by varying the etching times. Moreover, the expected opening angle of the Au split ring can be quantitatively predicted by knowing the height of the film all the way around an asymmetric PS ring (see Support Information).

It should be noted that it is challenging to obtain an opening angle of less than ~60° by using the templates in Figure 2b. This is because the lower part of the asymmetric rings is relatively flat when α is less than 60°. This is the general case for all asymmetric PS rings. However, the creation of very small gaps may be desired for generating structures that could be exploited in LSPR sensors or single molecule SERS measurements. To make a Au structure with a small gap, it is necessary to start from an asymmetric PS ring in which the height of the ring near the minimum point varies sharply. To do this, one can apply a large shear force and work under conditions of elevated annealing temperature.

Under such conditions, the equilibrium contact angle is approached. As such, the thickness of the ring is nearly uniform all the way around, but dips near the region of height minimum (Figure 7a,b). This was done by using a deflection angle of 18° as in Figure 4, but using a PS sample with a moleular weight of 18 kDa instead of 97.4 kDa to decrease the viscosity of the material. Therefore, the initial contact angle between the PS film and the PDMS wall was larger than θ_e all around the circle except near the point on the lowest side. We found that as long as the contact angle is larger than θ_e, the height of the capillary rise found for high annealing temperatures or low viscosity will eventually approach an identical value. This is limited only by the initial PS film thickness. As a result, the

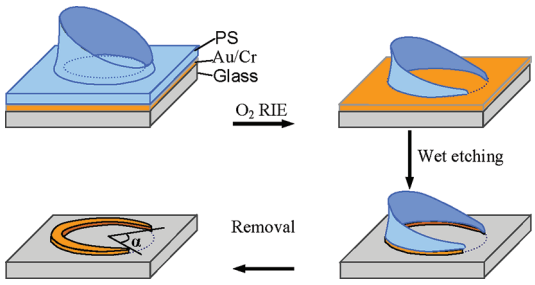

Figure 5. Schematic illustration of the procedure for fabricating Au split rings by using asymmetric PS rings, generated *via* dCFL, as templates. α is the opening angle of the Au split rings.

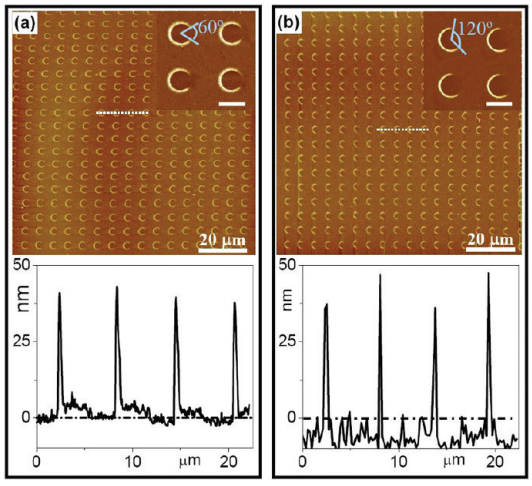

Figure 6. AFM images (100 μm × 100 μm) and corresponding line profiles of C-shaped Au rings obtained under etching times of (a) 45 s and (b) 65 s. The insets are the corresponding high-resolution AFM images (scale bars: 3 μm) showing opening angles of ~60° and ~120°, respectively.

asymmetry of the PS rings is confined to the region near h_{min} (Figure 7a). Indeed, the line profile across the minimum region clearly shows a sharp dip (inset of Figure 7b), which offers the possibility to fabricate split rings with a small opening angle or gap. Figure 7 panels c and d show that this structure can be transferred to a 30 nm thick Au film to create structures with an opening angle of ~10° (gap size, 250 ± 60 nm). Even smaller gaps could probably be formed by further optimization.

The dCFL method can also be used to create asymmetric structures in conjunction with PDMS stamps that contain triangular or square-shaped pillars (Figure 8). It should be noted, however, that the direction of the applied shear force F_x is important as these objects have a lower degree of symmetry than circular structures. Specifically, the direction of the shear force can lead to an opening at the apex of a triangle or along one of its sides (Figure 8a,b). As can be seen, applying a shear force from the apex of a triangle toward one of the sides leads to a relatively small opening compared with applying the shear force from the opposite side. The ability to control the size of the

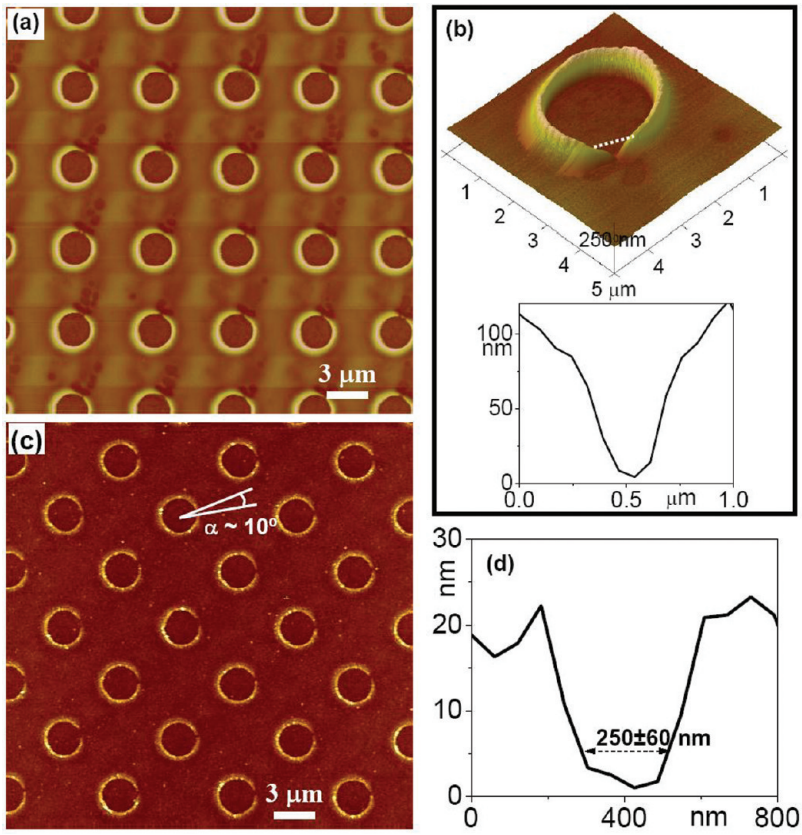

Figure 7. Fabrication of split rings with a small opening angle. (a) An AFM image (30 μm $\times$ 30 μm) of asymmetric PS rings fabricated under experimental conditions involving PS with M_w = 18 kDa, T = 130 °C, t = 30 min, and $m \approx 345$ g ($\varphi \approx 18°$). (b) A 3D AFM image of a PS ring (top) and its corresponding line profile (bottom). (c) An AFM image of the resultant Au split ring with an opening angle of ~10°. (d) A representative line profile of the opening gap in the AFM image from panel c.

opening by the shear force direction as well as variations in the applied load may have useful applications for creating devices with specific plasmonic properties. Analogous forces can also be applied when squared-shaped pillars are employed (Figure 8c,d). Such experiments suggest that a wide variety of structures could be generated using dCFL by using different shapes and varying the angle of the applied shear force. Of course, these structures can also be transferred to a Au film by RIE with resulting V, U, and C-shapes (Figure 9).

DISCUSSION

dCFL is a unique variation of soft lithography for fabricating asymmetric patterns that are not easily obtained by other methods. This technique exploits the interplay of several processes, including mechanical deflection, capillary rise, surface wetting, and etching, all of which could be used to tune the features of the patterned asymmetric structures. For example, different shapes can be generated by using different PDMS stamps. More importantly, by using a single PDMS stamp, asymmetric rings with various opening angles and shapes may be generated by simply changing the parameters in the experiment, which avoids the fabrication of a new PDMS stamp for each pattern.

Like other soft lithographic techniques, dCFL utilizes PDMS stamps to create micro/nanostructures. Therefore, it inherits the standard advantages of soft lithography. For example, the current method is applicable for generating patterns over large areas.[17,23] Indeed, uniform asymmetric rings could be generated over a sample of 1 cm^2. The area could be even larger if a larger PDMS stamp is employed. It should be noted that in order to obtain uniform asymmetric nanostructures over an entire sample, several precautions should be taken during the experiments. First, to make it contact the substrate tightly, the PDMS stamp should be only about 1 mm thick.[17] Second, the sample, including the PS film, PDMS stamp, and wedge, should be preheated to the annealing temperature of the dCFL process, which will eliminate the effects of thermal expansion during the heating process.[17,24] Third, to reduce the effect of contraction during the cooling process, the PDMS stamp should be released from the PS film only after cooling to the T_g of PS (~100 °C) upon completion of the dCFL process. Finally, to make the force applied to the substrate as uniform as possible, the contact point between the iron block and the glass slide on the wedge should be in the middle of the PDMS wedge/stamp.

Up until now, large-size split-rings have been fabricated by photolithography or ink jet printing methods.[25]

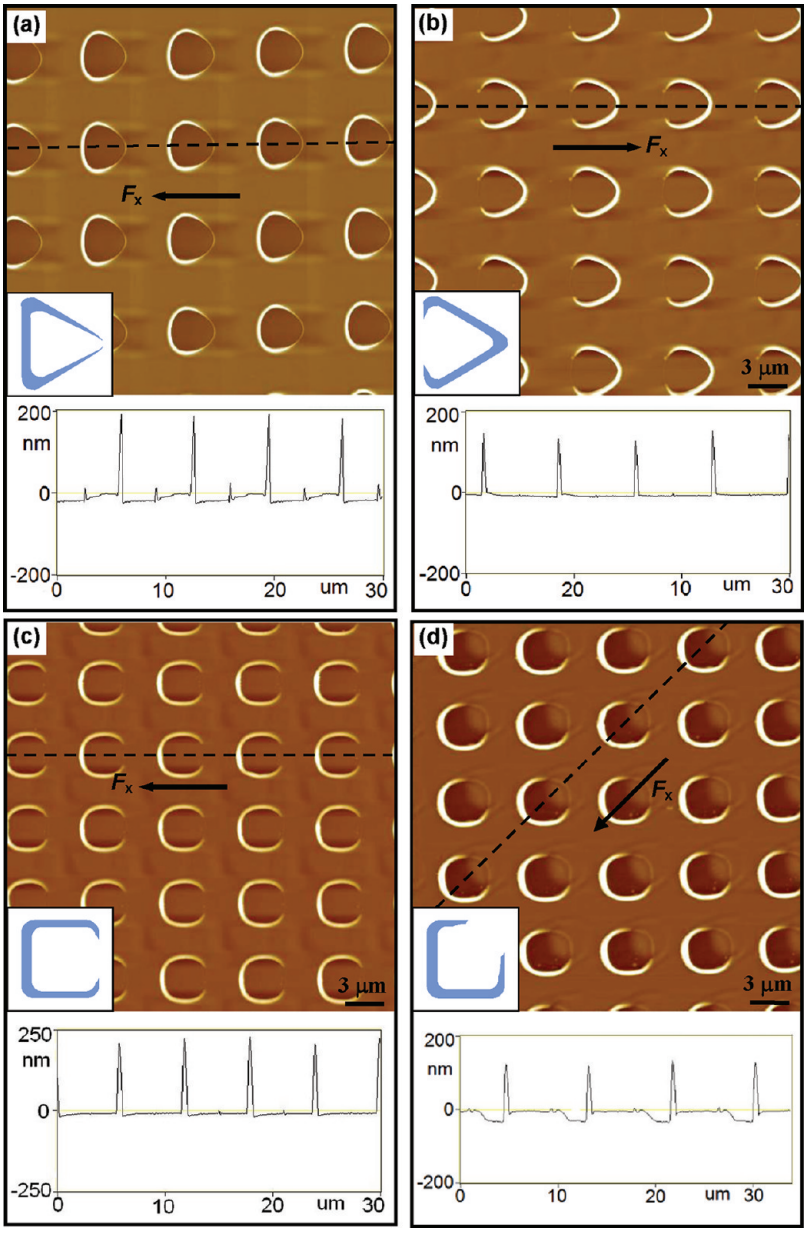

Figure 8. AFM images and the corresponding line profiles of asymmetric PS rings fabricated by using PDMS stamps with triangular (a,b) and square (c,d) pillars, respectively. The blue insets represent schematic depictions of each shape. The shear forces applied are indicated as the solid arrows in the images. Experimental conditions involve using PS with M_W = 97.4 kDa, T = 130 °C, and t = 30 min.

One drawback of these methods is that it is challenging to obtain submicrometer-sized line thicknesses for the split ring elements. By contrast, dCFL allows pattern feature sizes to be 100 nm or potentially less when using simple micrometer-sized PDMS patterns.[17] As shown in Figure 9a,b, the line width of the V-shaped split rings is ~100 nm. In addition, the PDMS stamp employed in this soft lithographic method is reusable. Moreover, no permanent deformation was observed in the PDMS stamp even after 30 uses for creating dCFL structures.

This technique is not limited to the PS materials used in this paper. Like other CFL techniques, it could be extended to other polymers and even different materials for additional applications. For example, polymers with functional groups could be used to generate asymmetric rings, which could be further functionalized by nanoparticles to obtain nanoparticle-based split-rings.[26] Alternatively, nanoparticle precursors could also be incorporated into the initial polymer thin film, which would allow one to obtain asymmetric rings composed of nanoparticles.[27] In addition to gold nanostructures, this technique could also allow for the fabrication of numerous metal and metal oxide nanostructures if the appropriate etching system is employed. This should

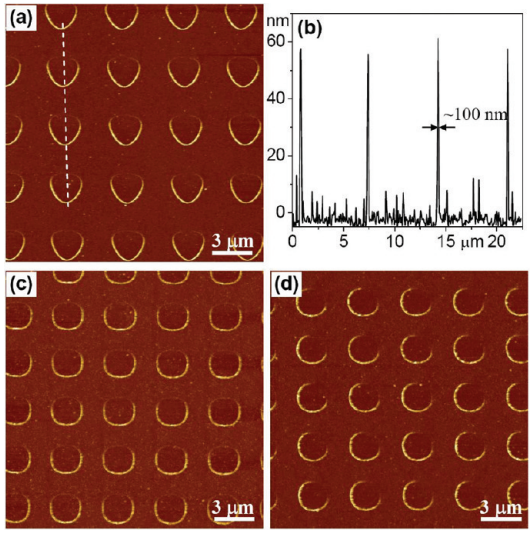

Figure 9. AFM images of Au split rings with (a) V, (b) U, and (c) C shapes obtained by using the PS rings from Figure 8 panels a, c, and d as templates, respectively. (b) A line profile for the dashed line in (a) showing that the feature width is ~100 nm.

enable the expansion of the application of split ring platforms.

Split rings fabricated by dCFL should have potential applications in plasmonics[28] and SERS,[29] as well as chemical and biosensors[1,8,9,30] due to their unique optical responses compared to symmetric structures. They may also be used as basic building blocks of metamaterials for applications in waveguides,[31] cloaks,[32] and negative refractive index materials.[3,6] Generally, uniform patterns over large areas are crucial for the practical applications of these platforms.[12,33−35] For example, terahertz metamaterials generally require a patterned area of ~1 cm^2.[36−39] For LSPR sensors, large-scale uniform nanostructures offer higher quality resonances and repeatable sensitivity.[12,34] The patterns fabricated by dCFL should meet these requirements in most cases. Also, the optical responses of split rings are known to be strongly dependent on their geometry, material, and size. This is significant, as optical responses ranging from the visible and infrared to the terahertz and microwave regions can be required for different purposes. With the methods provided herein, we have already generated split-ring elements in the size range from 500 nm to 100 μm (see Supporting Information).

CONCLUSIONS

We have demonstrated a new, simple, and cost-effective approach for generating asymmetric polymer rings. This new variant of CFL opens up a simple route to the generation of anisotropic geometric structures in a planar array-based format. The fabrication technique requires only a PDMS stamp and subsequent reactive ion etching. The formation of asymmetric polymer structures by dCFL is attributed to the asymmetric wetting of the polymer melt along the deflected PDMS pillars induced by the shear force. The opening angle of the PS rings could be varied by changing the annealing temperature, annealing time, and molecular weight of the sample. Moreover, opening angles in Au could be further controlled by changing the etching time. Since split structures follow the geometry of the PDMS pillars, this method allows one to fabricate shapes of almost arbitrary shape provided one makes chrome masks with the desired features. This technique could be readily extended to fabricate macro-, micro-, and nanosized anisotropic structures of various polymers and metals/metal oxides, which may find application in a wide range of fields.

METHODS

Materials. Photoresist (Shipley 1813) and photoresist development solution were obtained from Microchem Corp (MA). Glass coverslides (No. 2, 2 cm × 2 cm) were obtained from VWR (West Chester, PA). Samples of 50 nm gold (Au) films on 5 nm chromium (Cr) were prepared on the glass slides by metal evaporation (BOC Edwards Auto 306 metal evaporation chamber). 1*H*,1*H*,2*H*,2*H*-Perfluorodecyltrichlorosilane (FTS) was obtained from Alfa Aesar. Polydimethylsiloxane (PDMS, Sylgard 184) and its curing agent were obtained from Dow Corning. Polystyrene (PS) with four different molecular weights (M_w = 6.4, 18.1, 97.4, and 213.6 kDa) was purchased from Scientific Polymer Products, Inc. (Ontario, NY). $Fe(NO_3)_3 \cdot 9H_2O$ and thiourea were bought from Fluka.

Fabrication of PDMS Stamps. PDMS patterns were fabricated by standard photolithography. The square array patterns were formed using contact lithography with chrome masks containing circular, square, and triangular features (Image Technology, Palo Alto, CA). The circular features generally had 3 μm diameters, while the sides of the triangles and squares, were 4 and 3 μm, respectively. All elements were arrayed with 6 μm periodicity except for the triangular elements, which were arrayed with 7 μm periodicity. To make a post array pattern in PDMS, positive photoresist (PR) (shipley 1813) was first spin-coated on planar glass cover slides (2 cm × 2 cm) cleaned by piranha solution with a 70/30 (v/v) ratio of concentrated H_2SO_4 and 30% H_2O_2. (Caution: piranha solution is highly corrosive and reacts violently with organic matter.) The PR film was soft- baked at 115 °C for 1 min. To ensure a tight contact between the PR film and the chrome mask, the edges of the PR-covered glass slide were cut off before UV exposure. Subsequently, the PR film was exposed to UV light and developed. The size of the patterned PR sample was *ca.* 1 cm × 1 cm. Next, the exposed glass substrate with the PR pattern was exposed to FTS vapor for 1 h in an enclosed container. This rendered the surface more hydrophobic and ensured easy removal of the subsequently poured PDMS from the mold. PDMS was introduced from a 10:1 mixture of the polymer and a cross-linking agent followed by degassing in vacuum. After curing at 65 °C for 3 h, the PDMS stamp was removed from the mold, washed with acetone to remove any PR residue, and immersed in toluene for 2 h to remove uncross-linked PDMS molecules. The stamp was then allowed to dry in air. The thickness of the PDMS stamp was ~1 mm. This value ensured sufficient flexibility in the subsequent capillary force lithography process. PDMS stamps with three different shapes

(circular, square, and triangular) were fabricated as shown in Supporting Information, Figure S1.

Deflected Capillary Force Lithography (dCFL). A PS solution in toluene (10 mg/mL) was first filtered through a syringe filter with a 0.2 μm polytetrafluoroethylene (PTFE) membrane (Acrodisc CR 13 mm). PS thin films were spin-coated onto the Au-coated glass substrates at 3000 rpm for 30 s. The PS films were further baked at 110 °C for 10 min to remove the residual solvent, resulting in a ~50 nm thick film. The PDMS stamp and PS film were then separately heated to the desired temperature and brought into conformal contact to initiate capillary force lithography. A preheating step lasting 20 min was used to ensure uniform temperature. Next, a PDMS wedge with a glass slide was placed onto the PDMS stamp and an iron block was bridged between the hot plate and the wedge (Figure 1b). It should be noted that a microscope glass slide (1 mm in thickness) was placed on the PDMS wedge in order to avoid local deformation of the PDMS wedge and to ensure that a uniform force was applied onto the PDMS stamp. The film was annealed at a temperature above the glass transition temperature of PS for 30 min. The PDMS stamp was released from the PS substrate after cooling to the T_g of PS (~100 °C). This led to the formation of PS split rings over areas of ~1 cm ×1 cm (Supporting Information, Figure S2).

Fabrication of Au Split-Rings. Asymmetric PS rings were transferred to the underlying Au film by using the PS rings as templates. The substrate was first exposed to O_2 for RIE (60 W, 250 mTorr, 20 sccm O_2). This was done for 40−100 s to remove the residual PS layer. Subsequently, the substrate was immersed in absolute ethanol for 30 min in order to remove any possible oxide layer resulting from the uncured PDMS molecules.[17] The Au layer was etched in an aqueous solution of $Fe(NO_3)_3 \cdot 9H_2O$ (20 mM) and thiourea (30 mM), adjusted to pH 2.0 by HCl, with moderate shaking for 8 min at room temperature. Finally, the substrate was treated in an O_2 plasma to remove residual PS.

Characterization. PDMS stamps were imaged with an optical microscope (Witec Alpha300) and a scanning electron microscope (SEM, JEOL JSM-7500F). The PS film thickness was determined by measuring the depth of a scratch created by a needle using atomic force microscopy (AFM, Nanoscope IIIa, Veeco-Digital Instruments). The PS ring structures and the Au rings were examined by AFM. All AFM experiments were performed under tapping mode conditions. The error bars in this paper were based on measurements from at least two randomly chosen spots on each sample and a total of at least two samples were used in all cases.

Acknowledgment. We thank the Norman Hackerman Advanced Research Project (NHARP, 010366-0040-2009) from the Texas Higher Education Coordinating Board and the Office of Naval Research (N00014-08-0467) for funding and A. Wan for optical imaging.

Supporting Information Available: Optical and SEM images of PDMS stamps and large-area asymmetric PS rings, details regarding estimation of the deflection angle, effects of applied forces, effects of molecular weight of PS and annealing temperature, and applicability of dCFL for smaller and larger feature sizes. This materials is available free of charge *via* the Internet at http://pubs.acs.org.

REFERENCES AND NOTES

1. Cubukcu, E.; Zhang, S.; Park, Y.-S.; Bartal, G.; Zhang, X. Split Ring Resonator Sensors for Infrared Detection of Single Molecular Monolayers. *Appl. Phys. Lett.* **2009**, *95*, 043113.
2. Xu, Q.; Bao, J.; Rioux, R. M.; Perez-Castillejos, R.; Capasso, F.; Whitesides, G. M. Fabrication of Large-Area Patterned Nanostructures for Optical Applications by Nanoskiving. *Nano Lett.* **2007**, *7*, 2800–2805.
3. Shelby, R. A.; Smith, D. R.; Schultz, S. Experimental Verification of a Negative Index of Refraction. *Science* **2001**, *292*, 77–79.
4. Shumaker-Parry, J. S.; Rochholz, H.; Kreiter, M. Fabrication of Crescent-Shaped Optical Antennas. *Adv. Mater.* **2005**, *17*, 2131–2134.
5. Yen, T. J.; Padilla, W. J.; Fang, N.; Vier, D. C.; Smith, D. R.; Pendry, J. B.; Basov, D. N.; Zhang, X. Terahertz Magnetic Response from Artificial Materials. *Science* **2004**, *303*, 1494–1496.
6. Soukoulis, C. M.; Kafesaki, M.; Economou, E. N. Negative-Index Materials: New Frontiers in Optics. *Adv. Mater.* **2006**, *18*, 1941–1952.
7. Bukasov, R.; Shumaker-Parry, J. S. Highly Tunable Infrared Extinction Properties of Gold Nanocrescents. *Nano Lett.* **2007**, *7*, 1113–1118.
8. Lahiri, B.; Khokhar, A. Z.; De La Rue, R. M.; McMeekin, S. G.; Johnson, N. P. Asymmetric Split Ring Resonators for Optical Sensing of Organic Materials. *Opt. Express* **2009**, *17*, 1107–1115.
9. Clark, A. W.; Glidle, A.; Cumming, D. R. S.; Cooper, J. M. Plasmonic Split-Ring Resonators as Dichroic Nanophotonic DNA Biosensors. *J. Am. Chem. Soc.* **2009**, *131*, 17615–17619.
10. Liu, G. L.; Lu, Y.; Kim, J.; Doll, J. C.; Lee, L. P. Magnetic Nanocrescents as Controllable Surface-Enhanced Raman Scattering Nanoprobes for Biomolecular Imaging. *Adv. Mater.* **2005**, *17*, 2683–2688.
11. Linden, S.; Enkrich, C.; Wegener, M.; Zhou, J.; Koschny, T.; Soukoulis, C. M. Magnetic Response of Metamaterials at 100 Terahertz. *Science* **2004**, *306*, 1351–1353.
12. Gwinner, M. C.; Koroknay, E.; Fu, L.; Patoka, P.; Kandulski, W.; Giersig, M.; Giessen, H. Periodic Large-Area Metallic Split-Ring Resonator Metamaterial Fabrication Based on Shadow Nanosphere Lithography. *Small* **2009**, *5*, 400–406.
13. Lipomi, D. J.; Kats, M. A.; Kim, P.; Kang, S. H.; Aizenberg, J.; Capasso, F.; Whitesides, G. M. Fabrication and Replication of Arrays of Single- or Multicomponent Nanostructures by Replica Molding and Mechanical Sectioning. *ACS Nano* **2010**, *4*, 4017–4026.
14. Xu, Q.; Rioux, R. M.; Dickey, M. D.; Whitesides, G. M. Nanoskiving: A New Method To Produce Arrays of Nanostructures. *Acc. Chem. Res.* **2008**, *41*, 1566–1577.
15. Gao, L.; Lin, L.; Hao, J.; Wang, W.; Ma, R.; Xu, H.; Yu, J.; Lu, N.; Wang, W.; Chi, L. Fabrication of Split-Ring Resonators by Tilted Nanoimprint Lithography. *J. Colloid Interface Sci.* **2011**, *360*, 320–323.
16. Suh, K. Y.; Kim, Y. S.; Lee, H. H. Capillary Force Lithography. *Adv. Mater.* **2001**, *13*, 1386–1389.
17. Bruinink, C. M.; Peter, M.; Maury, P. A.; de Boer, M.; Kuipers, L.; Huskens, J.; Reinhoudt, D. N. Capillary Force Lithography: Fabrication of Functional Polymer Templates as Versatile Tools for Nanolithography. *Adv. Funct. Mater.* **2006**, *16*, 1555–1565.
18. Vega, M.-J.; Seveno, D.; Lemaur, G.; Adao, M.-H.; De Coninck, J. Dynamics of the Rise around a Fiber: Experimental Evidence of the Existence of Several Time Scales. *Langmuir* **2005**, *21*, 9584–9590.
19. Wu, S. Surface and Interfacial Tensions of Polymers, Oligomers, Plasticizers, and Organic Pigments. In *Polymer Handbook*; Brandrup, J., Immergut, E. H., Grulke, E. A., Eds.; John Wiley and Sons: New York, 1999; pp VI/525, VI/531, VI/537.
20. Bezuglyi, B. A.; Tarasov, O. A.; Fedorets, A. A. Modified Tilting-Plate Method for Measuring Contact Angles. *Colloid J.* **2001**, *63*, 668–674.
21. Schoen, I.; Hu, W.; Klotzsch, E.; Vogel, V. Probing Cellular Traction Forces by Micropillar Arrays: Contribution of Substrate Warping to Pillar Deflection. *Nano Lett.* **2010**, *10*, 1823–1830.
22. Fowkes, F. M.; Harkins, W. D. The State of Monolayers Adsorbed at the Interface Solid—Aqueous Solution. *J. Am. Chem. Soc.* **1940**, *62*, 3377–3386.
23. Suh, K. Y.; Lee, H. H. Capillary Force Lithography: Large-Area Patterning, Self-Organization, and Anisotropic Dewetting. *Adv. Funct. Mater.* **2002**, *12*, 405–413.
24. Bruinink, C. M.; Peter, M.; de Boer, M.; Kuipers, L.; Huskens, J.; Reinhoudt, D. N. Stamps for Submicrometer Soft

Lithography Fabricated by Capillary Force Lithography. *Adv. Mater.* **2004**, *16*, 1086–1090.
25. Takano, K.; Kawabata, T.; Hsieh, C.-F.; Akiyama, K.; Miyamaru, F.; Abe, Y.; Tokuda, Y.; Pan, R.-P.; Pan, C.-L.; Hangyo, M. Fabrication of Terahertz Planar Metamaterials Using a Super-Fine Ink-Jet Printer. *Appl. Phys. Express* **2010**, *3*, 016701.
26. Baek, Y.-K.; Yoo, S. M.; Kang, T.; Jeon, H.-J.; Kim, K.; Lee, J.-S.; Lee, S. Y.; Kim, B.; Jung, H.-T. Large-Scale Highly Ordered Chitosan-Core Au-Shell Nanopatterns with Plasmonic Tunability: A Top-Down Approach to Fabricate Core−Shell Nanostructures. *Adv. Funct. Mater.* **2010**, *20*, 4273–4278.
27. Park, M.; Hyun, D. C.; Kim, J.; Kim, Y. S.; Jeong, U. Dewetting-Induced Formation of Periodic Dot Arrays of Polymer/Au Composites by Capillary Force Lithography. *Chem. Mater.* **2010**, *22*, 4166–4174.
28. Sheridan, A. K.; Clark, A. W.; Glidle, A.; Cooper, J. M.; Cumming, D. R. S. Fabrication and Tuning of Nanoscale Metallic Ring and Split-Ring Arrays. *J. Vac. Sci. Technol., B* **2007**, *25*, 2628–2631.
29. Clark, A. W.; Cooper, J. M. Nanogap Ring Antennae as Plasmonically Coupled SERRS Substrates. *Small* **2011**, *7*, 119–125.
30. Driscoll, T.; Andreev, G. O.; Basov, D. N.; Palit, S.; Cho, S. Y.; Jokerst, N. M.; Smith, D. R. Tuned Permeability in Terahertz Split-Ring Resonators for Devices and Sensors. *Appl. Phys. Lett.* **2007**, *91*, 062511.
31. Marques, R.; Martel, J.; Mesa, F.; Medina, F. Left-Handed-Media Simulation and Transmission of EM Waves in Subwavelength Split-Ring-Resonator-Loaded Metallic Waveguides. *Phys. Rev. Lett.* **2002**, *89*, 183901.
32. Schurig, D.; Mock, J. J.; Justice, B. J.; Cummer, S. A.; Pendry, J. B.; Starr, A. F.; Smith, D. R. Metamaterial Electromagnetic Cloak at Microwave Frequencies. *Science* **2006**, *314*, 977–980.
33. Soukoulis, C. M.; Linden, S.; Wegener, M. Negative Refractive Index at Optical Wavelengths. *Science* **2007**, *315*, 47–49.
34. Zhao, J.; Frank, B.; Burger, S.; Giessen, H. Large-Area High-Quality Plasmonic Oligomers Fabricated by Angle-Controlled Colloidal Nanolithography. *ACS Nano* **2011**, *5*, 9009–9016.
35. Henzie, J.; Barton, J. E.; Stender, C. L.; Odom, T. W. Large-Area Nanoscale Patterning: Chemistry Meets Fabrication. *Acc. Chem. Res.* **2006**, *39*, 249–257.
36. Chen, H.-T.; Padilla, W. J.; Zide, J. M. O.; Gossard, A. C.; Taylor, A. J.; Averitt, R. D. Active Terahertz Metamaterial Devices. *Nature* **2006**, *444*, 597–600.
37. Chen, Z. C.; Hong, M. H.; Dong, H.; Gong, Y. D.; Lim, C. S.; Shi, L. P.; Chong, T. C. Parallel Laser Microfabrication of Terahertz Metamaterials and Its Polarization-Dependent Transmission Property. *Appl. Phys. A: Mater. Sci. Process.* **2010**, *101*, 33–36.
38. Tao, H.; Amsden, J. J.; Strikwerda, A. C.; Fan, K.; Kaplan, D. L.; Zhang, X.; Averitt, R. D.; Omenetto, F. G. Metamaterial Silk Composites at Terahertz Frequencies. *Adv. Mater.* **2010**, *22*, 3527–3531.
39. Chen, Z. C.; Han, N. R.; Pan, Z. Y.; Gong, Y. D.; Chong, T. C.; Hong, M. H. Tunable Resonance Enhancement of Multilayer Terahertz Metamaterials Fabricated by Parallel Laser Micro-Lens Array Lithography on Flexible Substrates. *Opt. Mater. Express* **2011**, *1*, 151–157.